Conversion of $[(^tBuCH_2)_2TaN]_5$ to Cubic TaN: Related Syntheses, EHMO Calculations, and MAS and Spin Echo ^{15}N NMR Spectroscopies

Mark M. Banaszak Holl, Peter T. Wolczanski,* Davide Proserpio, Anthony Bielecki,† and David B. Zax

Cornell University, Baker Laboratory, Department of Chemistry, Ithaca, New York 14853

Received January 19, 1996. Revised Manuscript Received June 14, 1996⊗

The conversion of pentamer $[(^tBuCH_2)_2TaN]_5$ (**2**) and ammonia to cubic $TaN_{0.8}$ (**5**) proceeds via precipitate $1/n[TaC_{1.41}H_{3.90}N_{1.90}]_n$ (**3**) and amorphous TaN (**4**). Precursors other than $(^tBuCH_2)_3Ta{=}CH^tBu$ (**1**) and NH_3, which provided **2**, such as $Ta(NMe_2)_5$ (**7**) and NH_3, $(Me_2N)_3Ta{=}N^tBu$ (**9**) and NH_3, also afforded **5**. Extended Hückel molecular orbital calculations were conducted to examine the electronic changes that appear upon oligomerization of hypothetical Me_2TaN to $(Me_2TaN)_\infty$, as a model for pentamer **2** formation. The relationship between pentamer **2** and the remaining nitrides, **3**−**5** was probed via magic angle spinning (MAS) and spin-echo solid-state ^{15}N NMR experiments that probe the local environments of the various nitrogen atoms. In combination with ^{15}N-labeling studies, the spin-echo spectra were used in an effort to analyze the possibility of a direct relationship between the 2-dimensional Ta_2N_2 "squares" of the pentamer (**2**) and the 3-dimensional Ta_4N_4 "cubes" of the ultimate product, cubic $TaN_{0.8}$ (**5**).

Introduction

The recent resurgence of materials[1] and solid-state[2] chemistry has prompted interest in new methodologies[3−5] for the preparation of refractory metal oxides, carbides, and nitrides.[6] Conventional methods of synthesizing solid-state materials involve high reaction temperatures, especially those requiring diffusion of elemental mixtures, conditions that tend to restrict the number and types of compounds that can be prepared.[7] Whereas oxidic compounds are not greatly limited by the severity of typical reaction conditions, the diversity of other ceramic materials is certainly constrained.

Transition-metal nitrides possess free energies of formation that are dramatically less favorable than corresponding oxides, principally because of the tremendous strength of the N≡N bond (227 kcal mol^{-1}) relative to O_2 (119 kcal mol^{-1}). As a consequence, the preparation of $[MN_n]_\infty$ from the respective elements is often entropically disfavored at the high temperatures necessary to ensure sufficient diffusion rates.[8] Since problems in the synthesis and processing of nitride-based compounds have limited their scope and hampered their implementation in current techologies, molecular precursor methods are currently being explored. To take full advantage of this technique, the relationship between precursor complex and the solid phase(s) must be understood,[9−11] perhaps through analyses of the intermediate stages of the conversion.

Scheme 1 summarizes previous work pertaining to the synthesis of metastable, cubic TaN_{1-x} via ammonolysis of a molecular precursor:[12−14] (1) treatment of $(^tBuCH_2)_3Ta{=}CH^tBu$ (**1**) with 5.0 equiv of NH_3 at 20 °C (11 h) in the absence of light provided pentamer $[(^tBuCH_2)_2TaN]_5$ (**2**), which was isolated as an ammonia

† Bruker Instruments, Inc., Boston, MA.

⊗ Abstract published in *Advance ACS Abstracts,* August 15, 1996.

(1) (a) Robinson, A. L. *Science* **1986**, *233*, 25−27. (b) *Sci. Am.* **1986**, *255*, 50−203. (c) Canby, T. Y.; O'Rear, C. *Natl. Geogr.* **1989**, *176*, 746−781.

(2) DiSalvo, F. J. *Science* **1990**, *247*, 649−655.

(3) (a) Interrante, L. V., Casper, L. A., Ellis, A. B., Eds. *Materials Chemistry: An Emerging Discipline*: ACS Series 245; American Chemical Society: Washington, DC, 1995. (b) Barron, A. R., Fishman, G. S., Fury, M. A., Hepp, A. F., Eds. *Covalent Ceramics II: Non-Oxides*; Elsevier: New York, 1994; Materials Research Society Symposium Proceedings, Vol. 327. (c) Laine, R. M., Ed. *Transformation of Organometallics into Common and Exotic Materials: Design and Activation*; NATO Advanced Science Institute Series; Martinus Nijhoff: Dordrecht, Holland, 1988. (d) Rao, C. N. R.; Gopalakrishnan, J. *New Directions in Solid State Chemistry*; Cambridge University Press; Cambridge, UK, 1986; pp 116−124.

(4) (a) Narula, C. K. *Ceramic Precursor Technology and Its Applications*; Marcel Dekker, Inc.: New York, 1995. (b) Lee, B. I.; Pope, E. J. A. *Chemical Processing of Ceramics*; Marcel Dekker, Inc.: New York, 1994. (c) Zelinski, B. J. J., Brinker, C. J., Clark, D. E., Ulrich, D. R., Eds. *Better Ceramics Through Chemistry IV*; Elsevier: New York, 1990; Materials Research Society Symposium Proceedings, Vol. 180. (d) Mackenzie, J. D.; Ulrich, D. R., Eds. *Ultrastructure Processing of Advanced Ceramics*; John Wiley & Sons: New York, 1988.

(5) (a) Brinker, C. J.; Scherer, G. W. *Sol-Gel Science: The Physics and Chemistry of Sol-Gel Processing*; Academic Press: San Diego, 1990. (b) Hench, L. L.; West, J. K. *Chemical Processing of Advanced Materials*; John Wiley & Sons: New York, 1992. (c) Hench, L. L.; West, J. K. *Chem. Rev.* **1990**, *90*, 33−72. (d) Livage, J.; Henry, M.; Sanchez, C. *Prog. Solid State Chem.* **1988**, *18*, 259−342.

(6) (a) Toth, L. E. *Transition Metal Carbides and Nitrides*; Academic Press: New York, 1971. (b) Johansen, H. A. Recent Development in the Chemistry of Transition Metal Carbides and Nitrides. In *Survey of Progress in Chemistry*; Scott, A. F., Ed.; Academic Press: New York, 1977; Vol. 8, pp 57−81.

(7) (a) West, A. R. *Solid State Chemistry and its Applications*; Wiley-Interscience: New York, 1984. (b) Cheetham, A. K., Day, P., Eds. *Solid State Chemistry Techniques*; Clarendon Press: Oxford, 1987.

(8) Elder, S. H.; DiSalvo, F. J.; Topor, L.; Novrotsky, A. *Chem. Mater.* **1993**, *5*, 1545−1553.

(9) Rouxel, J. *Acc. Chem. Res.* **1992**, *25*, 328−336.

(10) Isobe, K.; Yagasaki, A. *Acc. Chem. Res.* **1993**, *26*, 370−376.

(11) MacInnes, A. N.; Power, M. B.; Barron, A. R. *Chem. Mater.* **1993**, *5*, 1344−1351.

(12) Banaszak Holl, M. M. Ph.D. Thesis, Cornell University, 1991. An annotated program simulating lattice degradation of TaN, and a spin-echo pulse program written for a Bruker 300 MSL NMR spectrometer by Anthony Bielecki of Bruker Instruments, Inc., are included herein.

(13) Banaszak Holl, M. M.; Kersting, M.; Pendley, B. D.; Wolczanski, P. T. *Inorg. Chem.* **1990**, *29*, 1518−1526. EHMO calculations used the parameters and methods described herein.

S0897-4756(96)00034-8 CCC: $12.00

Scheme 1

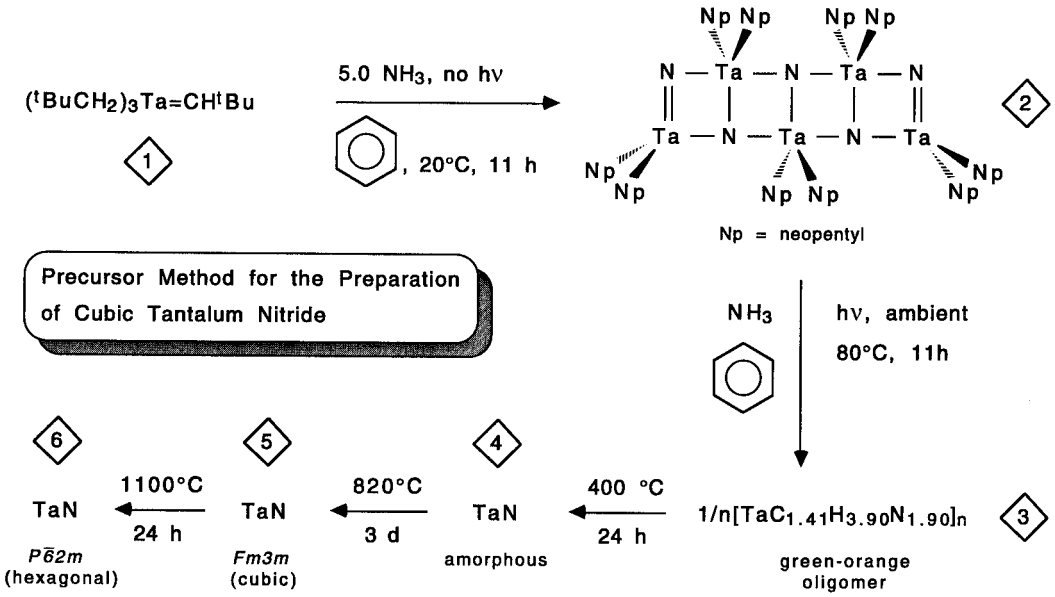

adduct, $[(^tBuCH_2)_2TaN]_5 \cdot NH_3 \cdot 2C_7H_8$ (**2**·NH_3·$2C_7H_8$);[14] (2) continued ammonolysis[15–19] at 80 °C for 11 h in the presence of ambient light[13] produced a green-orange precipitate, $1/n[TaC_{1.41}H_{3.90}N_{1.90}]_n$ (**3**); (3) thermolysis of **3** at 400 °C (24 h) generated amorphous TaN (**4**); (4) annealing at 820 °C (1 atm of Ar) for 3 days afforded cubic TaN_{1-x} (**5**, $Fm3m$, a = 4.300(2) Å, crystallite diameter ≥200−250 Å).[13,20–24] According to the phase diagram of Politis,[25] hexagonal TaN ($P\bar{6}2m$)[26] and Ta_2N nitrides are expected under the conditions employed, and the formation of $Fm3m$ TaN requires a nitrogen pressure. If the phase diagram, compiled from various independent studies, is assumed to be accurate, this solution precursor method accesses cubic TaN_{1-x} (**5**) under conditions (820 °C, 1 atm of Ar) that clearly implicate its formation as a kinetic (i.e., metastable) product. As a check, thermolysis of $Fm3m$ TaN_{1-x} (**5**) at 1100 °C for 24 h (1 atm of Ar) produced hexagonal TaN_{1-x} (**6**, $P\bar{6}2m$), as suggested by the phase diagram. Figure 1 depicts the hexagonal ($P\bar{6}2m$)[26] and cubic ($Fm3m$, rock salt) structures of TaN_{1-x}.[22,23] Upon inspection of these illustrations, the structural relationship between pentamer $[(^tBuCH_2)_2TaN]_5$ (**2**) and cubic TaN_{1-x} is clearly apparent.[12,14]

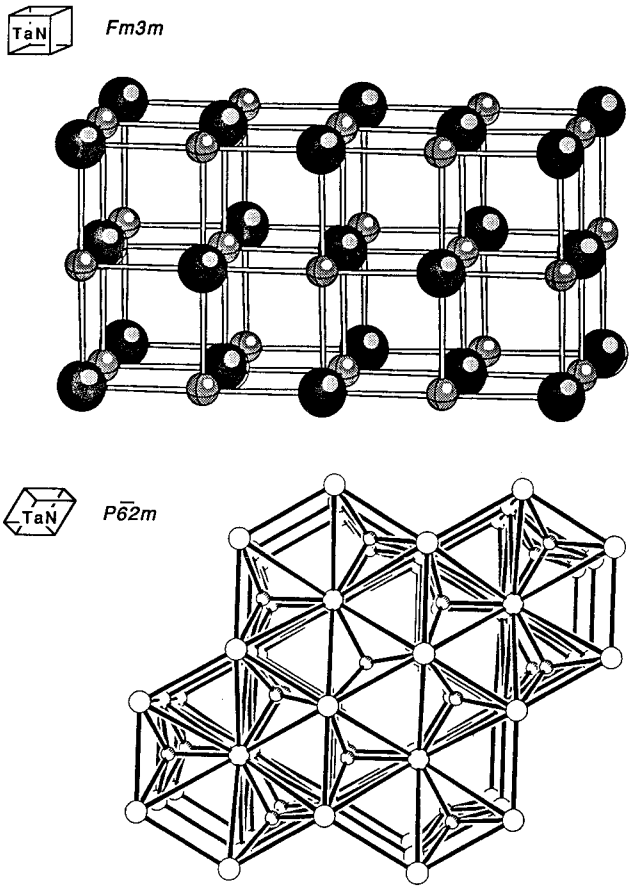

Figure 1. Depictions of hexagonal ($P\bar{6}2m$) and cubic ($Fm3m$)-TaN.

(14) Banaszak Holl, M. M.; Wolczanski, P. T.; Van Duyne, G. D. *J. Am. Chem. Soc.* **1990**, *112*, 7989−7994. In this paper, the structure of hexagonal TaN is represented as $P6/mmm$, but current interpretation of XRD data suggests that $P\bar{6}2m$ is best. Arguments presented are consistent with either space group.

(15) For preceramic nitride powders generated from metal halides and ammonia, see: (a) Brown, G. M.; Maya, L. *J. Am. Ceram. Soc.* **1988**, *71*, 78−82. (b) Maya, L. *Inorg. Chem.* **1987**, *26*, 1459−1462. (c) Maya, L. *Inorg. Chem.* **1986**, *25*, 4213−4217. (d) Maya, L. *Mater. Res. Soc. Proc.* **1986**, *73*, 401−406. (e) Brown, G. M.; Maya, L. *Inorg. Chem.* **1989**, *28*, 2007−2010.

(16) For preceramic nitride powders generated from metal amides and ammonia, see: (a) Fowles, G. W. A.; Pollard, F. H. *J. Chem. Soc.* **1952**, 4938−4942. (b) Fowles, G. W. A.; Pleass, C. M. *J. Chem. Soc.* **1957**, 1674−1681. (c) Fowles, G. W. A.; Nicholls, D. *J. Chem. Soc.* **1958**, 1687−1690. (d) Fowles, G. W. A.; Osborne, B. P. *J. Chem. Soc.* **1959**, 2275−2279.

(17) For the recent formation of TiN via ammonolysis of $Ti(NMe_2)_4$, see: Seyferth, D.; Mignani, G. *J. Mater. Sci. Lett.* **1988**, *7*, 487−488.

(18) For the recent formation of LnN (Ln = lanthanide) via ammonolysis of $Ln\{N(SiMe_3)_2\}_3$, see: LaDuca, R. L.; Wolczanski, P. T. *Inorg. Chem.* **1992**, *31*, 1313−1315.

(19) For related CVD of groups 4 and 5 nitrides via chemically similar ammonolyses, see: (a) Fix, R. M.; Gordon, R. G.; Hoffman, D. M. *Chem. Mater.* **1993**, *5*, 614−619. (b) Fix, R. M.; Gordon, R. G.; Hoffman, D. M. *Chem. Mater.* **1991**, *3*, 1138−1148. (c) Fix, R. M.; Gordon, R. G.; Hoffman, D. M. *Chem. Mater.* **1990**, *2*, 235−241. (d) Fix, R. M.; Gordon, R. G.; Hoffman, D. M. *J. Am. Chem. Soc.* **1990**, *112*, 7833−7835. (e) Fix, R. M.; Gordon, R. G.; Hoffman, D. M. *Mater. Res. Soc. Proc.* **1990**, *168*, 357−362.

(20) From XRD, the crystallite diameter, $t = 0.9\lambda/B \cos\theta_B$, where $B^2 = B_M^2 - B_S^2$ (B_M = half-maximum line width (in radians) at $2\theta_B$, B_S = half-maximum line width (in radians) of a line near $2\theta_B$ corresponding to a standard).

(21) *Powder Diffraction File*; International Centre for Diffraction Data: Swarthmore, PA, 1988.

(22) For general references on the structure of tantalum nitrides, see: (a) Terao, N. *Jpn. J. Appl. Phys.* **1971**, *10*, 248−259. (b) Schönberg, N. *Acta Chem. Scand.* **1954**, *8*, 199−203.

This article describes various attempts to elucidate the relationship between pentamer **2** and the remaining nitrides, **3**−**5**. Magic angle spinning (MAS) and spin-echo solid-state ^{15}N NMR experiments[27] that probe the local environments of the various nitrogen atoms are described; in combination with ^{15}N-labeling studies, the latter was used in an effort to analyze the possibility of a direct relationship between the 2-dimensional Ta_2N_2 "squares" of the pentamer (**2**) and the 3-dimensional Ta_4N_4 "cubes" of the ultimate product, cubic TaN_{1-x} (**5**).

Results and Discussion

Synthesis and Characterization of Cubic TaN_{1-x}. While the previous syntheses of compounds **1**−**5** are readily adaptable to the preparation of ^{15}N-labeled materials from $^{15}NH_3$,[12−14] alternatives were explored. As a control experiment, (^{t}BuCH$_2$)$_3$Ta=CH^{t}Bu (**1**)[28] was allowed to react in the solid state with flowing ammonia at 25 °C. The immediate formation of an oil was noted, and a silver-red solid formed upon heating to 800 °C. In contrast to Scheme 1, a mixture of *Fm*3*m* TaN_{1-x}, Ta_3N_5, and other products was produced according to analysis by X-ray powder diffraction (XRD).

Other precursors were used in the successful production of cubic TaN (**5**), but lower quality nitride was generated. Treatment of $Ta(NMe_2)_5$ (**7**)[29] with excess NH_3 in hexane at −78 °C immediately liberated Me_2NH and precipitated a yellow powder (**8**, eq 1). Annealing the powder at 400 °C (24 h) resulted in a ≫14% weight loss and a jet black, amorphous solid. An additional ∼9.4% weight loss was observed upon further heating at 800 °C (3 days, eq 2) and cubic TaN_{1-x} again formed (*Fm*3*m*, a = 4.310(2) Å, albeit with ∼5% unidentifiable crystalline impurities. Given the weight loss data, **8** must be considered to possess ∼1 NMe_2 fragment per tantalum atom, and can be roughly formulated as "$1/n[(Me_2N)Ta(NH_2)_a(NH)_bN_c]_n$" (**8**, $a + 2b + 3c = 4$).

$$\underset{\mathbf{7}}{Ta(NMe_2)_5} \xrightarrow[\text{hexane, } -78\rightarrow 25\ ^\circ C]{NH_3\ (1\ atm)} \sim 4Me_2NH + \underset{\mathbf{8}}{\text{“}1/n[(Me_2N)Ta(NH_2)_a(NH)_bN_c]_n\text{”}} \quad (1)$$

$$\mathbf{8} \xrightarrow[24\ h]{400\ ^\circ C} \underset{\mathbf{4}}{TaN\ (\text{amorphous})} \xrightarrow[3\ days]{800\ ^\circ C} \underset{\mathbf{5}}{TaN_{1-x}\ (Fm3m)} \quad (2)$$

Similar results were obtained when $(Me_2N)_3Ta{=}N^tBu$ (**9**)[30] was exposed to 1 atm of NH_3 in hexane at 20 °C. After 4 h, formation of a yellow precipitate was noted, and removal of the volatiles resulted in a glassy solid. Annealing at 400 °C (24 h) provided an amorphous, shiny black material accompanied by a ∼36% weight loss; subsequent thermolysis for 42 h at 600 °C produced no further weight loss, and additional annealing at 950 °C for 4 days afforded clean, but poorly crystalline TaN_{1-x}. According to the weight loss study, a substantial number of Me_2N and ^{t}BuN functionalities remain bound to the tantalums in the yellow precipitate. Since the the tantalum nitride prepared from **7** or **9** was of lesser quality than **5** prepared via **1** according to Scheme 1, only the latter material and its relevant precursors (**2**−**4**) were subjected to further mechanistic scrutiny. From a practical standpoint, $Ta(NMe_2)_5$ (**7**)[29] may be a more desireable precursor to cubic TaN_{1-x} (**5**) because of its ready synthesis and higher tantalum percentage, assuming the application did not depend greatly on the purity of the nitride generated.

The cubic TaN_{1-x} (**5**) generated via the precursor method in Scheme 1 was determined to be nitrogen deficient, but some ambiguity in the actual stoichiometry persists. XRD cannot distinguish nitrogen content or ordering in the lattice because the scattering of X-rays is dominated by the tantalums. Various samples of **5** were subjected to spectrophotometric Kjeldahl analysis to determine the nitrogen content. The values obtained suggested that the correct formulation for **5** was $TaN_{0.8}$, but the degradation did not occur smoothly. Although boiling $H_3PO_4/SnCl_2$ was found to dissolve **5**,[31,32] the resulting mixture was heterogeneous, with gray-black coloration indicative of an incomplete reaction, and thus the nitrogen number is believed to be a lower limit (i.e., $TaN_{\geq 0.8}$). Alternative methods, including boiling HF, failed to decompose **5**. In similar fashion, the stoichiometry of commercial hexagonal (Aldrich, $P\bar{6}2m$) tantalum nitride was determined to be $TaN_{0.95}$.

The magnetic susceptibility of $TaN_{0.8}$ (**5**), as measured by Faraday balance, manifested weak diamagnetic behavior from 255 K (-3.2×10^{-8} emu/g) to 100 K (-2.4×10^{-8} emu/g). Below 100 K, the sample exhibited a paramagnetic tail that could not be fit using the Curie−Weiss law. At approximately 4 K, part of the sample became superconducting, but the magnitude of χ was not great enough to reflect a bulk transition, and hence its origin remains questionable.

Solid-State MAS ^{15}N NMR Studies of Nitrides. Each nitride in Scheme 1 was prepared from 98%

(23) For information regarding cubic TaN and related carbides, see: (a) Gatterer, J.; Dufek, G.; Ettmayer, P.; Kieffer, R. *Monatsh. Chem.* **1975**, *106*, 1137−1147. (b) Petrunin, V. F.; Sorokin, N. I. *Izv. Akad. Nauk SSR, Neorg. Mater.* **1982**, *18*, 2005−2008. (c) Boiko, L. G.; Popova, S. V. *JETP Lett.* **1970**, *12*, 70−71. (d) Kieffer, R.; Ettmayer, P.; Freundhofmeier, M.; Gatterer, J. *Monatsh. Chem.* **1971**, *102*, 483−485. (e) Matsumoto, O.; Konuma, M.; Kanzaki, Y. *J. Less-Common Met.* **1978**, *60*, 147−149.

(24) (a) Wittmer, M. *Appl. Phys. Lett.* **1980**, *36*, 456−458. (b) Wittmer, M. *Appl. Phys. Lett.* **1980**, *376*, 540−542.

(25) Politis, C. *Contemp. Inorg. Mater., Proc. Ger.-Yugosl. Meet., 3rd*; Petzow, G., Huppmann, W. J., Eds.; Dr. Riederer-Verlag Gmbh: Stuttgart, Germany, 1978; pp 152−157.

(26) (a) Christensen, A. N.; Lebech, B. *Acta Crystallogr.* **1978**, *B34*, 261−263. (b) Petrunin, V. F.; Sorokin, N. I. *Izv. Akad. Nauk SSR, Neorg. Mater.* **1982**, *18*, 2005−2008. (c) Brauer, G.; Zapp, K. H. *Z. Anorg. Allg. Chem.* **1954**, *277*, 129−139.

(27) (a) Abragam, A. *Principles of Nuclear Magnetism*; Oxford, Clarenden Press: London, 1961. (b) Slichter, C. P. *Principles of Magnetic Resonance*, 3rd ed.; Springer-Verlag: New York, 1990. (c) Fyfe, C. A. *Solid State NMR for Chemists*; C. F. C. Press: Guelph, Ontario, 1983. (d) Sanders, J. K. M.; Hunter, B. K. *Modern NMR Spectroscopy*; Oxford University Press: New York, 1987. (d) Drago, R. S. *Physical Methods in Chemistry*; W. B. Saunders Co.: Philadelphia, 1977.

(28) Schrock, R. R.; Fellmann, J. D. *J. Am. Chem. Soc.* **1978**, *100*, 3359−3370.

(29) Bradley, D. C.; Thomas, I. M. *Can. J. Chem.* **1962**, *40*, 1355−1360. **Warning**: the procedure presented in this paper yields a highly explosive powder (presumably finely divided $LiNMe_2$) if rigorously followed; free Me_2NH must be present for the reaction to proceed safely.

(30) Nugent, W. A. *Inorg. Chem.* **1983**, *22*, 965−969.

(31) Bollman, D. H. *Anal. Chem.* **1972**, *43*, 887−888.

(32) Combustion analyses of **3** may not be wholly accurate due to the stability of the nitrides and carbides of tantalum. For TaN (**5**), the modified Kjeldahl analysis was used because commercial combustion analyses proved to be irreproducible. On the basis of the modified Kjeldahl analysis, assuming all "vacancies" are filled with carbon, the maximum possible %C is 1.23.

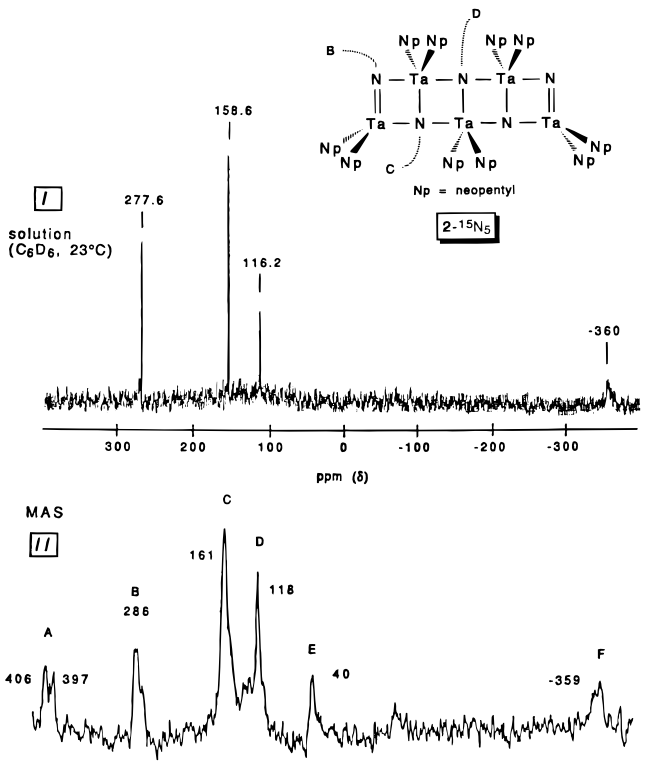

Figure 2. MAS ^{15}N NMR spectrum (**II**) of $[(^tBuCH_2)_2Ta^{15}N]_5 \cdot {}^{15}NH_3 \cdot 2C_7H_8$ (**2**-$^{15}N_5 \cdot {}^{15}NH_3 \cdot 2C_7H_8$) as compared to the solution (C_6D_6, 23 °C) spectrum (**I**) of $[(^tBuCH_2)_2Ta^{15}N]_5$ (**2**-$^{15}N_5$) and ammonia (δ −360). Spectrum **II** was acquired using direct polarization of the ^{15}N nuclei.

$^{15}NH_3$ and subjected to analysis by magic angle spinning (MAS) ^{15}N NMR spectroscopy in order to probe plausible spectral correlations.[33] Spectra were acquired using direct polarization of the ^{15}N nucleus and magic angle spinning (MAS),[27] but the high density of the materials studied in this work (∼12−15 g/cm^3) often prevented spin rates above 3−5 kHz. Where possible, assignments are based upon comparison with molecular nitride clusters.[34,35] Solid spectra were initially referenced to solid NH_4Cl, but are reported referenced to neat nitromethane for correlation to solution data.[36] The line widths of each sample were found to be very sensitive to phasing of the spectrum, the acquisition parameters used, and manner in which the data were Fourier transformed; therefore, they should be considered as qualitative indicators of sample environment.

1. Pentamer [(ᵗBuCH₂)₂TaN]₅ (2). The MAS ^{15}N solid-state NMR spectrum (**II**, Figure 2) of $[(^tBuCH_2)_2Ta^{15}N]_5 \cdot {}^{15}NH_3 \cdot 2C_7H_8$ (**2**-$^{15}N_5 \cdot {}^{15}NH_3 \cdot 2C_7H_8$) was assigned through comparison to the previously acquired solution ^{15}N NMR spectrum (**I**), which contained a ∼2:2:1 set of nitride resonances at δ 277.6, 158.6, and 116.2.[14] From the intensities, the middle, T-shaped nitride is attributed to **D** (δ 118), while regions **B** (δ 286) and **C** (δ 161) are the remaining two- and three-coordinate nitrides. Since **C** is nearest in chemical shift to **D**, it is ascribed to the two interior 3-coordinate nitrides. Regions **E** (δ 40) and **F** (δ −359) are tentatively assigned as coordinated and free ammonia (e.g., NH_3(l); δ −380), respectively, although the breadth of the latter is somewhat puzzling; lattice bound NH_3 was presumably generated due to the heating incurred during acquisition and may indicate some degradation. The solution spectrum of **2**-$^{15}N_5 \cdot {}^{15}NH_3 \cdot 2C_7H_8$, while reflecting the C_{2v} symmetry of **2**, also exhibited a broad signal (δ −360) for free NH_3 undergoing exchange with bound ammonia.[14] Site differences and the bound NH_3 render the "ends" of the ladder complex (**2**-$^{15}N_5 \cdot {}^{15}NH_3 \cdot 2C_7H_8$) inequivalent in the solid state, hence some of the line-width broadness in **B**, **C**, and **D** may be attributed to subtle differences in chemical shift. Region **A** (δ 406, 397) remains an enigma, since analogous resonances have not been observed in solution, and the shifts were inconsistent with possible sidebands.

2. Precipitate 1/*n*[TaC$_{1.41}$H$_{3.90}{}^{15}$N$_{1.90}$]$_n$ (3-^{15}N). In Figure 3, the MAS ^{15}N NMR spectrum of oligomeric precipitate $1/n[TaC_{1.41}H_{3.90}{}^{15}N_{1.90}]_n$ (**3**-^{15}N, **III**) is compared with those of its precursor and successor nitrides. The majority of nitride in **3**-^{15}N is assigned as three-coordinate (δ 118, **D**, ∼54%), yet additional two or three-coordinate nitrides are present (δ 225 ppm, **G**, ∼4%) and no obvious spectral features remain in regions **A** or **B**. Region **E′** could be assigned as bound ammonia as in **II** (**E**) but is best attributed to four- to six-coordinate nitride (δ 13, −71 ppm, ∼10%).[34,35] The features in region **H** (δ −234, −306 ppm, ∼15%) correspond to amides,[34,35] while the second largest peak in the spectrum (δ −358 ppm, region **F**, ∼17%) is most consistent with free ammonia as in **II**, or with ammonium (cf. NH_4Cl (s); δ −341). Using these assignments, the N:H compositional ratio of ∼1.2−1.6 roughly correlates with the elemental analysis, since much of the hydrogen is expected to be bound to residual carbon. For example, if all the remaining carbon is present as neopentyl, the precipitate can be formulated as $1/n[Ta(Np)_{0.28}H_{0.80}N_{1.90}]_n$. In this formulation the sum of the tantalum and hydrogen valences (+5.80) is nearly equivalent in magnitude to the sum of the neopentyl and nitrogen valences (−5.98), thereby adding credence to this depiction. Both types of analysis agree that the nitrogen in the sample should be predominantly (>50%) in the form of nitride. Imide functionalities expected in the −100 to −200 ppm range[34,35] are apparently absent, suggesting that disproportionation to N^{3-} and NH_2^- and scavenging by NH_3 to yield two amides are significant pathways. Amide and ammonia ligands should prefer binding sites on the exterior of an aggregate, and hence the cross-linking of $[TaN]_n$ ladders may produce a nitride-based oligomer with minimal order, one whose surface is coated with NH_3 and NH_2 groups.

3. Amorphous Ta^{15}N (4-^{15}N). The MAS ^{15}N NMR spectrum (**IV**) of $Ta^{15}N$ (**4**-^{15}N) is shown relative to **3**-^{15}N (**III**) and $Ta^{15}N_{0.8}$ (**5**-^{15}N, **V**) in Figure 3. The majority of the signal is concentrated in regions **D** and **E′**, assigned to 3- and 4−6-coordinate nitride, respectively. Region **D**, centered at δ 119, corresponds to somewhat less than ∼50% of the sample, suggesting that **4**-^{15}N contains a significant number of 3-coordinate nitrides

(33) For a related ^{15}N NMR study of AlN production via precursor ammonolysis, see: Baker, R. T.; Bolt, J. D.; Reddy, G. S.; Roe, C.; Staley, R. S.; Tebbe, F. N.; Vega, A. J. *Mater. Res. Soc. Symp. Proc.* **1988**, *121*, 471−476.

(34) (a) von Philipsborn, W.; Muller, R. *Angew. Chem., Int. Ed. Engl.* **1986**, *25*, 383−406. (b) Mason, J. *Chem. Rev.* **1981**, *81*, 205−227. (c) Mason, J. *J. Am. Chem. Soc.* **1991**, *113*, 24−26. (d) Mason, J. *Ibid.* **1991**, *113*, 6056−6062. (e) Gladfelter, W. L. *Adv. Organomet. Chem.* **1985**, *24*, 41−86.

(35) Banaszak Holl, M. M.; Wolczanski, P. T. *J. Am. Chem. Soc.* **1992**, *114*, 3854−3858 and references therein.

(36) Hayashi, S.; Hayamizu, K. *Bull. Chem. Soc. Jpn.* **1991**, *64*, 688−690.

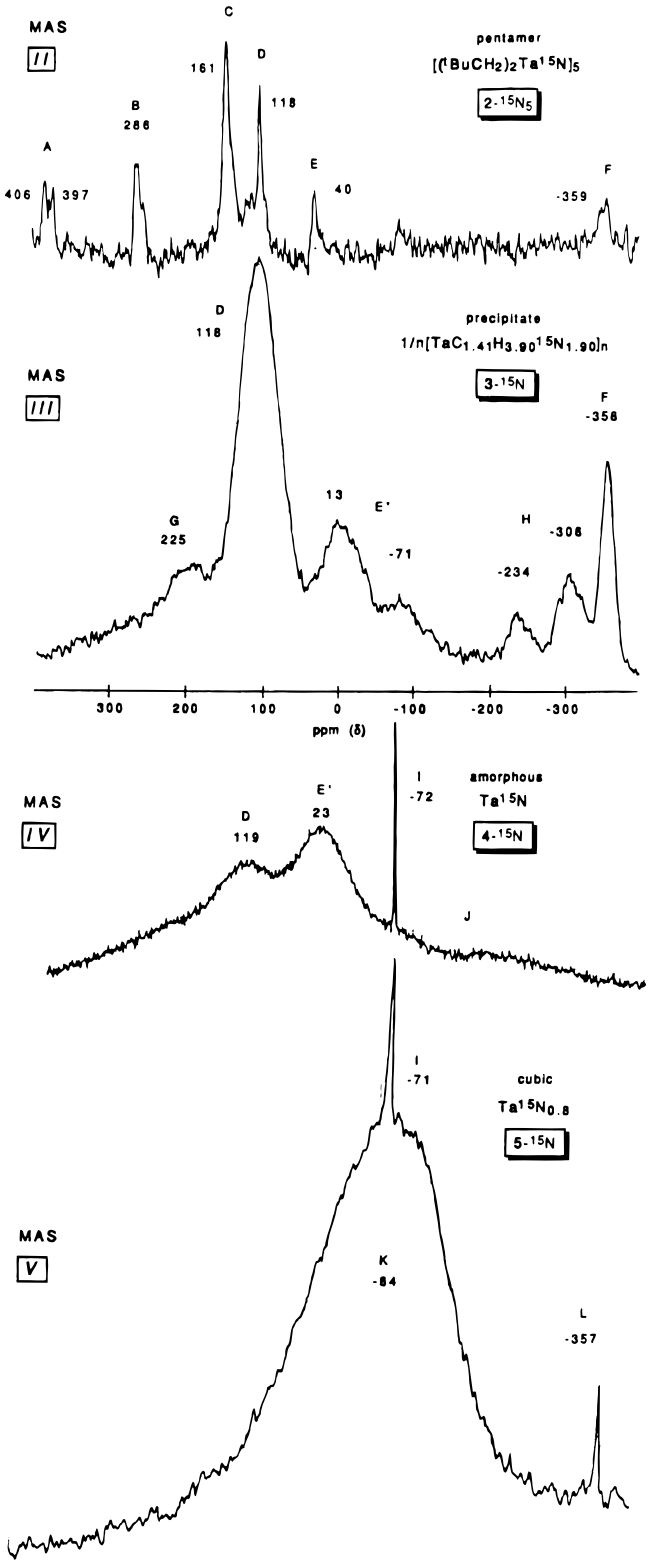

Figure 3. Solid-state ^{15}N NMR spectra of **2**-$^{15}N_5$·$^{15}NH_3$·$2C_7H_8$ (**II**), oligomeric precipitate $1/n[TaC_{1.41}H_{3.90}{}^{15}N_{1.90}]_n$ (**3**-^{15}N, **III**), amorphous $Ta^{15}N$ (**4**-^{15}N), and cubic $Ta^{15}N_{0.8}$ (**5**-^{15}N). Spectra were acquired using MAS and direct polarization of the ^{15}N nuclei.

even after annealing to 400 °C (24 h) and that the ladder motif of pentamer $[(^tBuCH_2)_2Ta^{15}N]_5$ (**2**-$^{15}N_5$) may persist. Region **E′**, centered at δ 23, has grown to >50% of the sample. The growth of absorptions in **E′** upon annealing is consistent with the formation of four- to six-coordinate nitrides via cross-linking of ladder units. The slight hump appearing in region **J** may correlate with low-coordinate imides but is most likely due to baseline instability.

While direct polarization ^{15}N NMR of **4**-^{15}N gave a substantial signal, acquisition using cross-polarization to protons gave no signal. Generally, when protons were present, cross polarization was found to increase the signal/noise by a factor of ~10, thus the absence of signal supports the contention that a minimal number of N−H bonds remain. The carbon content was also probed via MAS ^{13}C NMR using direct polarization and cross-polarization to protons. No signal was obtained, corroborating the stoichiometry previously addressed,[13] but it is realistic to assume that trace amounts of carbide (1−5% relative to N) cannot easily be observed by this technique.[23]

4. Cubic $TaN_{0.8}$ (5-^{15}N). MAS solid-state ^{15}N NMR was also used to study *Fm*3*m* $TaN_{0.8}$ (**5**-^{15}N, Figure 3, V). The vast majority of the sample consists of a very broad peak at ~δ −84 (**K**, $\nu_{1/2}$ = 6000 Hz, 98%). Two additional peaks comprised only ~2% of the sample and were comparatively sharp (δ −71 ppm, **I**, $\nu_{1/2}$ = 160 Hz; δ −357 ppm, **L**, $\nu_{1/2}$ =110 Hz). A spike similar to **I** occurs at δ −72 ppm for **4**-^{15}N (**IV**), and both are best considered artifacts of the data treatment. A separate sample of **5**-^{15}N prepared in the same fashion gave only the broad peak at δ −84 (**K**). The position of **L** is reminescent of the free NH_3 ascribed to resonance **F** in the spectra of pentamer $[(^tBuCH_2)_2TaN]_5$ (**2**-$^{15}N_5$, spectrum **II**) and precipitate $1/n[TaC_{1.41}H_{3.90}{}^{15}N_{1.90}]_n$ (**3**-^{15}N, spectrum **III**). It only represents ~1% of the sample and is attributed to NH_3 trapped within an N-site vacancy; the sharpness of the resonance would then be related to the rapid rotational motion of the trapped ligand.[27] Hydrolysis of trace amounts of **5**-^{15}N upon brief handling in air was expected based on the observation of oxide upon prolonged exposure.

The ~6000 Hz width of the primary peak at δ −84 (**K**) prompted consideration of several line-broadening mechanisms: (1) paramagnetism; (2) quadrupolar couplings;[37] (3) dipolar ("through space") couplings; (4) *J* couplings ("through-bond"); (5) chemical shift anisotropy; (6) chemical-shift inhomogeneity.[27] Since $TaN_{0.8}$ (**5**) is a weak diamagnet, paramagnetic line-broadening was considered unlikely**.** In principle, dipolar couplings and chemical shift anisotropy are removed by magic angle spinning since both have a $3\cos^2\theta - 1$ dependence. If the energy of the interaction is greater than or approximately equal to the spin rates obtained (3−5 kHz), the anisotropy will not be be fully removed. An approximation of the expected effect of dipolar coupling upon line width can be made by calculation of second moment expected for the peak.[27] Various estimates for *Fm*3*m* TaN, assuming either Gaussian or Lorentzian line shapes, revealed that such broadening is substantially less (<600 Hz) than the observed 6000 Hz line width. Second-order dipolar broadening will contribute to the line width but to a much lesser extent. *J* couplings could be of three types: $^{15}N-Ta-{}^{15}N$, $^{15}N-Ta-{}^{14}N$, or $^{181}Ta-{}^{15}N$. Model complexes containing $Ta-{}^{15}N$ bonds (e.g., **2**-$^{15}N_5$) have not manifested measurable coupling in solution (cf. $J(^{183}W-{}^{15}N)$ ~23 Hz),[38,39] nor has quadrupolar broadening proven to be an observ-

(37) Mueller, K. T.; Wu, Y.; Chmelka, B. F.; Stebbins, J.; Pines, A. *J. Am. Chem. Soc.* **1991**, *113*, 32−38 and references therein.
(38) Mason, J. *Multinuclear NMR*; Plenum Press: New York, 1987.

able factor, and two-bond J couplings for ^{15}N are typically less than 5 Hz.[34] Although solution- and solid-state J couplings are not rigorously equivalent, the expected magnitudes of these interactions are substantially less than required to rationalize the broadness observed in **K**.

Peak **K** is centered in a region expected for high-coordinate nitrides or μ_3-imides[34,35] and spans 300 ppm from relatively low-coordinate nitrides to amides. Consistent with nitrogen analyses, chemical shift inhomogeneity, caused principally by a manifold of nitrogen sites, is the major contributor to the line-broadening. Since analysis places the N content of **5** at ~80% of that pertaining to a perfect cubic lattice, the resulting nitrogen vacancies disrupt the local symmetry and create multiple sites. For example, a rough statistical analysis based on 80% occupancy of the nitrogen sites predicts that only ~7% of the nitrogens are surrounded by the ideal number (12) of next nearest neighbors, whereas ~21%, ~28%, ~23%, and ~13% contain one, two, three and four vacancies, respectively. Although peak **K** spans some 300 ppm, a large chemical shift dispersion is inherent to ^{15}N and is clearly evident from the above spectra. Even the nitride shifts of the pentamer $[(^tBuCH_2)_2Ta^{15}N]_5$ (**2**-^{15}N) differ by ~170 ppm.[14] Variation in the next-nearest-neighbor coordination sphere can significantly perturb the field about the core ^{15}N atom, thereby accounting for its breadth. These factors do not take into account possible tantalum vacancies, which will add to the disorder and resulting chemical shift dispersion in the system.

Other causes of asymmetry may also contribute substantially to the line broadening. A major cause could be the presence of tantalum vacancies, which change the coordination number about the core ^{15}N. The MAS spectra in Figure 3 are clear in indicating major chemical shift changes upon variation in the coordination number of nitrogen. The particle size of **5** (probably ~300−6000 Å in diameter, vide infra) may also contribute to line broadening. Assuming a spherical particle of diameter 300 Å for **5**-^{15}N, roughly ~5% of the nitrogens are on its exterior, and >10% are within 2 unit cells of the surface. If the exterior is irregular or the particle is nonspherical, as expected (vide infra), an even greater number of nitrogens will exist in regions that are clearly different than the interior of the particle and will manifest correspondingly disparate chemical shifts. In addition, a crystallite diameter of 200−250 Å has been estimated from the XRD data of **5**; therefore, although most particle sizes (i.e., >350 Å) may be sufficient to preclude substantial chemical shift inhomogeneity from surface perturbations, the interfacial region between crystallites may cause some broadening.

Structural Models. The correlations noted between stoichiometry, chemical analysis,[32] MAS ^{15}N NMR spectra, and chemical intuition are encouraging, particularly the general agreement pertaining to the types of nitrides present in the various samples. As more data for nitride, imide, and amide functionalities are obtained,[34,35] it should be possible to further refine and assess the limitations of the spectral assignments. However, there are enough data available to posit structural models of **3**−**5**.

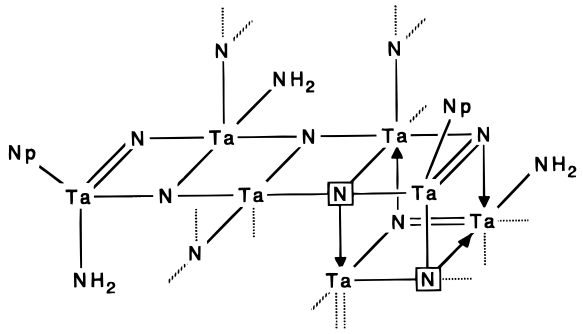

Figure 4. Structural model of $1/n[TaC_{1.41}H_{3.90}N_{1.90}]_n$ (**3**) based MAS ^{15}N NMR spectral features (**III**, Figure 3), elemental analysis, and stoichiometry.

1. Precipitate $1/n[TaC_{1.41}H_{3.90}N_{1.90}]_n$ (3). The model of $1/n[TaC_{1.41}H_{3.90}N_{1.90}]_n$ (**3**) illustrated in Figure 4 encompasses the MAS ^{15}N NMR spectral features (**III**, Figure 3), elemental analysis, and previously noted stoichiometric requirements.[13] A typical portion of the precipitate will contain 50−60% 3-coordinate nitrides, with the possibility of some 2-coordinate N^{3-} groups. In generating the structure, a basis of seven tantalum atoms, one 2-coordinate and seven 3-coordinate nitrides were used, and one complete pentamer unit has been kept intact. Two 4-coordinate nitrides (implied by **E′** in **III**, boxed in the Figure 4) help form a Ta_4N_4 cube via condensation with a portion of another ladder, while the two neopentyl groups that reflect the carbon content hinder growth in two directions. Several of the nitrides indicate other cross-links, and all of the tantalums are pictured in the +5 oxidation state, as previously discussed. Although it is possible that **3** contains reduced Ta sites, these sites should be scavenged by the oxidative addition of ammonia.

The three amides, again suggested by the NMR data, may result from cleavage of the neopentyl groups or from the NH_3 oxidative addition. The stoichiometry of the model structure is $1/n[TaC_{1.43}H_{4.0}N_{1.86}]_n$ (or $1/n[Ta(CH_2{}^tBu)_{0.29}H_{0.85}N_{1.86}]_n$), in remarkably good agreement with the elemental and product analyses. Formation of the structure is envisioned to occur through ammonia cleavage of Ta−Np groups and condensation of amide and nitride functionalities. Photolysis may aid this process by inducing elimination or abstraction reactions[40] that encourage swift attack at the metal center by NH_3, and precipitation occurs when solubility is lost due to extensive cross-linking.

2. Amorphous TaN (4). Previous weight loss measurements[13] taken upon thermolysis of **3** at 400 °C (24 h) to give amorphous TaN (**4**) are consistent with the elimination of neopentane, ammonia, 0.5 equiv of dihydrogen and 0.5 equiv of dinitrogen. Dinitrogen is necessarily generated due to reduction of the tantalums. Further condensation and the cross-linking of the ladders in **3** are proposed to occur simultaneously with the generation of the volatiles. As a consequence, the 4- to 6-coordinate region (**E′**) of the MAS ^{15}N NMR spectrum of **4** (**IV**) grows (>50%) at the expense of the 3-coordinate region (**D**), and only these two features are present, although the breadth of the resonances can easily

(39) Chisolm, M. H.; Hoffman, D. M.; Huffman, J. C. *Inorg. Chem.* **1985**, *24*, 796−797.

(40) Schrock, R. R. *J. Organomet. Chem.* **1976**, *122*, 209−225.

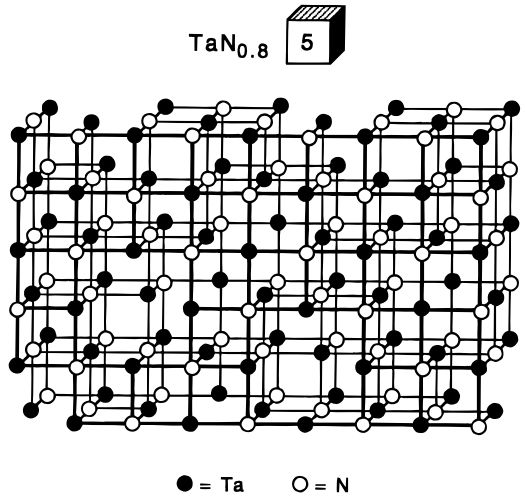

Figure 5. Model of $TaN_{0.8}$ (**5**), depicting a portion of its ~20% nitrogen-deficient lattice. The model assumes full tantalum occupancy.

accommodate small amounts of additional structural features or differing types of sites as discussed for cubic $TaN_{0.8}$ (**5**). The material, while uniform according to electron microscopy, is amorphous to XRD, and the amount of order is unknown.

3. Cubic $TaN_{0.8}$ (5). A representation of $TaN_{0.8}$ (**5**), depicting a portion of its nitrogen-deficient lattice, is illustrated in Figure 5. The XRD results reflect the requisite face-centered cubic lattice, but ~20% nitrogen vacancies are mandated by elemental analysis[32] and MAS ^{15}N NMR. Due to the N-atom vacancies and exterior sites, it is a rare instance when a N-atom is surrounded by a full complement of 12 nearest-neighbor nitrogens (statistically ~7%). The vacancies can also accommodate trapped ammonia, providing a plausible explanation for the spike observed in ^{15}N MAS NMR spectra of **5**-^{15}N (Figure 3, V, region **I**). This model was constructed *assuming 100% tantalum occupancy*, an occurrence that is suspect. Given the interpretation of the structure of amorphous TaN (**4**) above, it is conceivable that densification of the tantalum nitride upon annealing will introduce substantional irregularities in the tantalum lattice. Unfortunately, the number of tantalum vacancies is difficult to ascertain, especially in light of problems assessing the density of solid-state particulate matter. Since such metal vacancies undoubtedly exist, the conclusions reached on the basis of the ^{15}N MAS spectra of **5** are further justified. Furthermore, it is conceivable that a portion of the presumed vacancies are occupied by carbon derived from the neopentyl groups of the precursor. Unfortunately, such possibilities were difficult to assess with the analytical capabilities at hand.

EHMO Calculations of $[(^tBuCH_2)_2TaN]_5$ (2). The initial starting materials, $(^tBuCH_2)_3Ta{=}CH^tBu$ (**1**) and NH_3, have no predisposition to ultimately form either hexagonal or cubic lattices. However, pentamer $[(^tBuCH_2)_2TaN]_5$ (**2**) is geometrically related to *Fm*3*m* TaN, since its core is comprised of Ta_2N_2 squares that can be used to construct cubic tantalum nitride.[14] Extended Hückel molecular orbital (EHMO) calculations[13] were utilized to explore the electronic character of the oligomer.

EHMO calculations performed on $[Me_2TaN]_5$ (**2′**), a hypothetical model of $[(^tBuCH_2)_2TaN]_5$ (**2**), were compared to related $[Me_2TaN]_n$ ($n = 2 \rightarrow \infty$) oligomers and cubic TaN. The calculations show that $E_n - nE_1$ (E_1 is the total energy of a monomer unit, $Me_2Ta{\equiv}N$; E_n is the corresponding energy of $[Me_2TaN]_n$) decreases linearly with n, indicating that the addition of $Me_2Ta{\equiv}N$ to any chain length is equally favorable (~5 eV), as expected. More importantly, Figure 6 shows that $E_n/n - E_1$ approaches the value of an infinite chain, $[Me_2TaN]_\infty$, in rapid fashion. Specifically, the energy of a Me_2TaN unit in the pentamer has ~85% of the total stabilization it would possess in the infinite polymer; consequently, the electronic character of the pentamer *resembles an extended structure*, and orbitals critical to the stabilization of the pentamer are analogous to those of $[Me_2TaN]_\infty$. Figure 7 indicates that the parallel Ta−N overlap population (parallel indicating overlap in the plane of a planar ladder, i.e., π-type overlap) of 0.610 is within 2% of the value corresponding to an infinite chain, while the perpendicular Ta−N overlap population (perpendicular indicating overlap perpendicular to the plane of a planar ladder, i.e., pure π-type overlap) of 0.572 is only ~9% higher than that of $[Me_2TaN]_\infty$. Both are greater than the Ta−N overlap of cubic $TaN_{1.0}$, calculated to be 0.347, because the Ta−N distances of **2** (1.84−2.17 Å; 2.00 Å average) are significantly shorter than the 2.165 Å distance used for

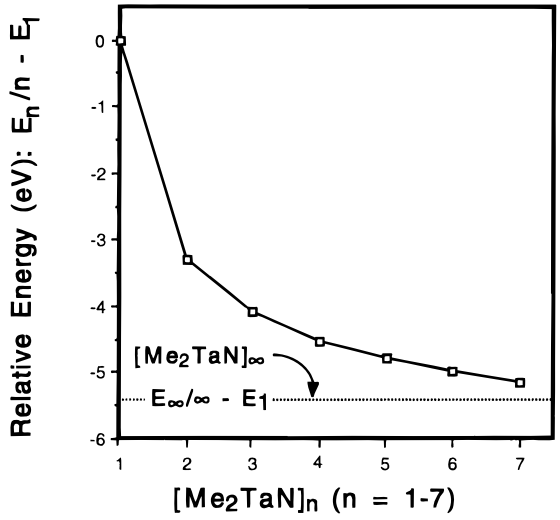

Figure 6. $E_n/n - E_1$ is shown to quickly approach that of an infinite chain, $[Me_2TaN]_\infty$. E_1 is the total energy of a monomer unit, $Me_2Ta{\equiv}N$; E_n is the corresponding energy of $[Me_2TaN]_n$.

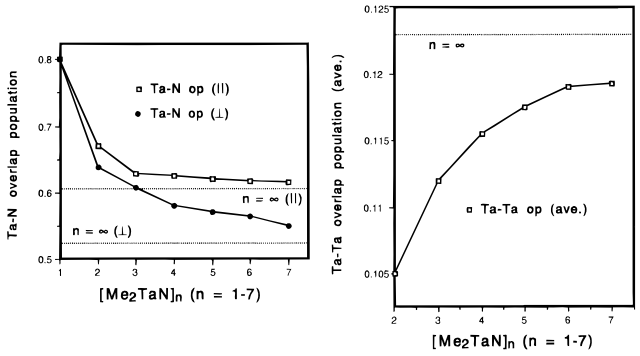

Figure 7. Ta−N (parallel indicating overlap in the plane of a planar ladder, i.e., π-type overlap; perpendicular indicating overlap perpendicular to the plane of a planar ladder, i.e., pure π-type overlap) and Ta−Ta overlap population of $[Me_2TaN]_n$ as a function of chain length.

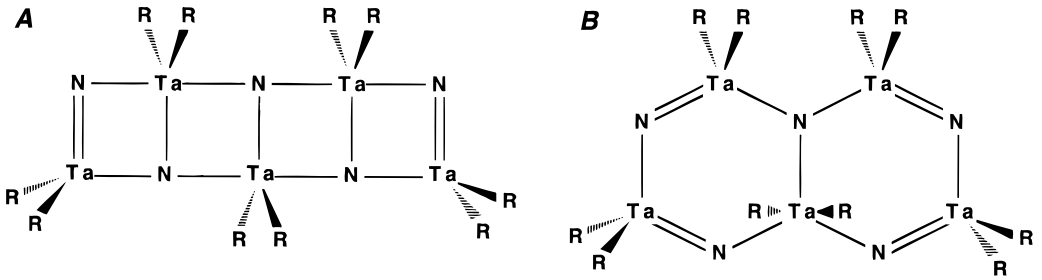

Figure 8. Valence bond structures for the ladder (**A**) and naphthalene-like (**B**) geometries of $[R_2TaN]_5$.

the latter. In addition, the overlap population between the tantalums quickly approaches the infinite limit, with $[Me_2TaN]_5$ (**2′**) having 95% of the Ta−Ta overlap of $[Me_2TaN]_\infty$. The Ta−Ta overlap of 0.117 for **2′** is significant and suggests that even in the all Ta(V) structure substantial metal−metal interaction is present, since the corresponding Ta−Ta overlap for cubic TaN is 0.083. Again, the longer Ta−Ta distances of TaN (3.06 Å), vs the 2.86−3.09 Å distances of **2**, correspond with the lower value of the former.

A calculation of the partial charges on the nitrogens of **2′** revealed that the 3-coordinate nitrides possess partial charges of −0.56 and −0.53, in comparison to a −0.41 value for the 6-coordinate nitride of cubic TaN. The values of the organometallic derivative are remarkably close to the solid-state Ta(III) compound, despite the Ta(V) oxidation state of the former. The tantalum partial charges in **2′** and cubic TaN (+0.41) reflect the disparate oxidation states, differing by ∼0.6. Apparently, the covalent character of the short Ta−N bonds in **2** lessens the ionic character of the bonds, because a calculation of **2′** with 2.165 Å Ta−N bond lengths led to significantly higher partial charges (−0.79 and −0.76) on the interior nitrogens. The electroneutrality principle of Pauling[41] is evident in the surprising similarites between oligomer and solid-state materials.

Figure 8 illustrates valance bond structures for $[R_2TaN]_5$ (**A**) and a naphthalene-like geometry (**B**). Calculations of **2′** in both configurations revealed that the pentameric ladder (**A**) is favored by ∼3.7 eV, an exceedingly high amount. A large portion of the energy difference arises from a notable destabilization of the **2′** HOMO as the Ta_2N_2 squares are being transformed into the edge-shared hexagons of **B**. The HOMO, primarily Ta−N π-bonding in **2′** and ∼0.37 eV above a cluster of σ-based orbitals, is converted into a molecular orbital with substantial Ta(central)−C antibonding character upon breaking the second and fourth rungs of the ladder. Evidently **B** falls far short of possessing the increased π-bonding necessary to overcome the strong σ- and π-interactions of the interior perpendicular Ta−N bonds. Whereas the Ta_2N_2 squares of **A** can be used to construct cubic TaN ($Fm3m$), the core of **B**, with its edge-shared hexagons and potential for trigonal coordination about each tantalum, contains certain structural elements of hexagonal TaN ($P\bar{6}2m$). The stability of **A** relative to **B** supports the premise that the Ta_2N_2 squares may remain intact during the course of $TaN_{0.8}$ (**5**) formation from **2** and that these subunits may direct the formation of metastable cubic TaN with respect to the thermodynamically favored hexagonal form.

Mechanistic Studies. The aforementioned synthesis of $Fm3m$ TaN (Scheme 1) at ambient pressure (1−100 atm below previous syntheses) and ∼1000 °C below the temperatures required for previous solid and thin-film preparations immediately poses the question of how and why the transformation is possible. The core of pentamer $[(^tBuCH_2)_2TaN]_5$ (**2**) is geometrically related to $Fm3m$ TaN, since it is comprised of Ta_2N_2 squares that can be used to construct cubic tantalum nitride. A trivial mechanism consists of reductive elimination of all neopentyl groups and subsequent condensation to generate the cubic lattice, yet the true microscopic steps are complicated and not directly observable. The reduction actually occurs after ammonolysis of almost all the neopentyl groups, according to various analyses and weight loss measurements. Despite these mechanistic limitations, it is still plausible that the pentamer core remains completely or partially intact during the conversion of **2** to $TaN_{0.8}$ (**5**). This possibility serves as the premise of a key mechanistic experiment involving spin-echo solid-state ^{15}N NMR spectroscopy.[27,42,43]

1. Concept. The solid-state MAS ^{15}N NMR spectra provide interesting information about the conversion of $[(^tBuCH_2)_2TaN]_5$ (**2**) to $TaN_{0.8}$ (**5**) but do not indicate whether the pentamer has remained intact during the conversion. The premise that an intact Ta_5N_5 fragment constitutes a building block for $TaN_{0.8}$ (**5**), and therefore serves as proof of a direct relationship between **2** and **5**, became the basis of the labeling experiment illustrated by Scheme 2. A mixture of 95% **2** and 5% ^{15}N-labeled pentamer, **2**-$^{15}N_5$ was dissolved to give a homogeneous solution. As in Scheme 1, NH_3 was added to generate the precipitate, followed by the thermal procedures yielding amorphous and cubic TaN. *Provided the Ta_5N_5 and $Ta_5{}^{15}N_5$ pentamers remain intact during the process*, these "pentamer-doped" products will possess *local concentrations* of ^{15}N, as the idealized precipitate **3**-$(^{15}N_5)_{0.05}$, amorphous nitride **4**-$(^{15}N_5)_{0.05}$, and cubic nitride **5**-$(^{15}N_5)_{0.04}$ portray in Scheme 2. For comparison, samples containing randomly distributed ^{15}N were prepared from $(^tBuCH_2)_3Ta{=}CH^tBu$ (**1**) and 95% NH_3/5% $^{15}NH_3$ in a control experiment. In this manner, the percent of ^{15}N in **2** was held at 5% in both

(41) Pauling, L. *The Nature of the Chemical Bond*, 3rd ed.; Cornell University Press: Ithaca, New York, 1960.

(42) (a) Lizak, M. J.; Gullion, T.; Conradi, M. S. *J. Magn. Reson.* **1991**, *91*, 254−260. (b) Elbaum, N. C.; Haw, J. F. *J. Magn. Reson.* **1991**, *91*, 199−203. (c) Kang, S.; Namboodin, M.; Fiat, D. *J. Magn. Reson.* **1991**, *93*, 1−11.

(43) (a) Carr, H. Y.; Purcell, E. M. *Phys. Rev.* **1954**, *94*, 630−638. (b) Gill, D.; Meiboom, S. *Rev. Sci. Instrum.* **1958**, *29*, 688−691.

Scheme 2

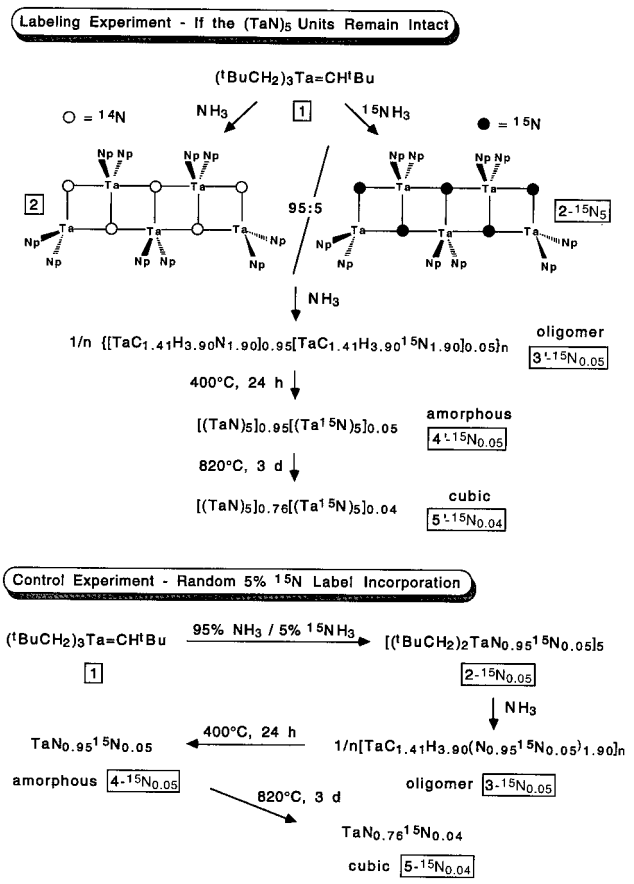

the pentamer-doped and random label experiments. The percent of ^{15}N doping was chosen somewhat arbitrarily based on rough estimates of localized vs random ^{15}N distribution; other percentages could also be used, and may ultimately prove necessary (vide infra). At 5%, the randomly doped samples also serve as a measure of the inherent line widths in each sample.

In practice, the annealing process (i.e., **3**→**5**) must require some N diffusion on the atomic scale, but this experiment would still evidence a direct relationship between **2** and the resulting solids provided the distribution of ^{15}N was not random. Although it is very unlikely that $Ta_5{}^{15}N_5$ pentamers would be completely retained in the conversion of **2** to **5**, smaller $Ta_n{}^{15}N_n$ ($1 < n < 5$) units, such as $Ta_2{}^{15}N_2$ squares or various $Ta_4{}^{15}N_4$ arrangements, would still provide a direct link to the precursor complex *as long as their concentration is greater than statistical.*

2. Confirmation of the Integrity of **2**-$^{15}N_5$ *upon Ammonolysis.* The labeling experiments are moot if the ammonolysis step that converts **2**-$^{15}N_5$ to **3** results in loss or significant dilution of the ^{15}N-label prior to formation of the precipitate. The formation of **3** from **2**-$^{15}N_5$ and 5.0 equiv of NH_3 was monitored via ^{15}N NMR. No evidence of $^{15}NH_3$ was detected, nor was any *preferential* ^{15}N loss from **2**-$^{15}N_5$ noted during its conversion to **3**. Since no increase in $^{15}NH_3$ was discerned by ^{15}N NMR at >90% conversion of **2**-$^{15}N_5$, the precipitate also does not undergo significant exchange with NH_3.

3. Unsuccessful Attempts to Measure ^{15}N *Distribution.* Oxidative degradations of **4′**-$^{15}N_{0.05}$ (10−50 mg) were initially used in an attempt to detect local concentrations of ^{15}N by mass spectrometry via nonstatistical ratios of $^{15}N_2/^{15}N^{14}N$. The experiments relied on the assumption of nearest neighbor nitrogen−nitrogen bond formation, and the expected isotopomer ratios were derived from computer simulations of lattice decomposition.[12] However, various experimental difficulties led to imprecise measurements, principally because of trace water contamination and spurious NO formation. Direct analysis of **4**/**4′**-^{15}N by FAB MS[44] yielded only peaks consistent with surface oxides. Apparently the ubiquitous oxide coat of the bulk nitrides was impervious to the FAB gun, despite bombardment of the sample for 20 min at a gun voltage of 10 keV.

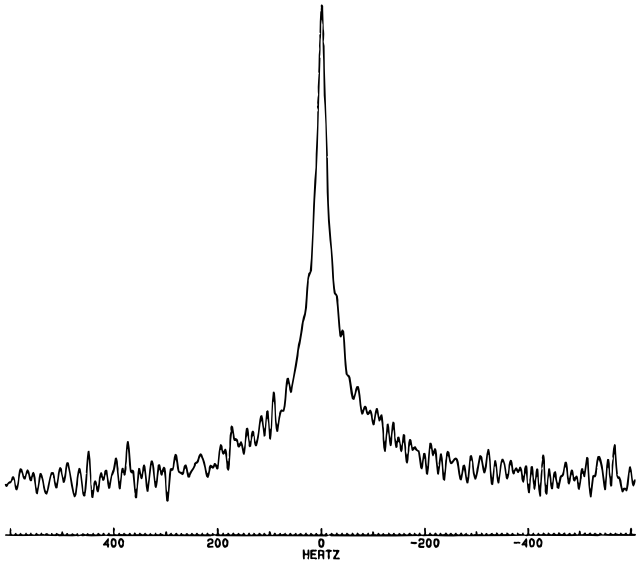

Figure 9. The spectrum of $Ta^{15}N_{0.8}$ (**5**-^{15}N) observed in a CPMG spin-echo sequence. For convenience, the signal can be fit to a pair of Lorentzian line shapes (LINESIM, Bruker Insturments) with full widths at half-height of ∼54 (∼80%) and ∼140 Hz (∼20%).

4. Spin-Echo Solid-State ^{15}N *NMR Analysis.* The spin-echo solid-state NMR experiment is noninvasive and can provide a direct measure of the local concentration of ^{15}N in the lattice.[27,42,43] Experimental drawbacks include the need for relatively large samples (250−500 mg), difficulties inherent in its execution, and ambiguities regarding interpretation of the resulting line widths. All spin-echo spectra were acquired using the Carr−Purcell−Meiboom−Gill (CPMG) sequence.[43] Where data are accumulated in each of the windows between the pulses, the resulting spectrum is dominated by the homonuclear direct dipolar and homonuclear J couplings, which tend to be localized phenomena (0−10 Å). Dipolar couplings have a $1/r^3$ distance dependence and J couplings tend to be limited to about five bonds. Broadening due to chemical shifts and couplings to other magnetic nuclei are largely suppressed, including those to ^{14}N. As a consequence, the spectral line widths measured in a CPMG experiment are primarily sensitive to the nearby distribution of distances to similar nuclear spins.

The spectrum of $Ta^{15}N_{0.8}$ (**5**-^{15}N) observed in a CPMG spin-echo sequence consists of a relatively sharp spike (∼80%) atop a broadened base (∼20%), as shown in Figure 9. For convenience, the line shape can be fit to

(44) Bruce, M. I.; Liddell, M. J. *Appl. Organomet. Chem.* **1987**, *1*, 191−226.

a pair of Lorentzian line shapes (LINESIM, Bruker Insturments) with full widths at half-height of ~54 and ~140 Hz. These should be construed not as separate resonances but as the spectrum arising from a large number of interacting homonuclear couplings. The data provide confirmation that the ~6000 Hz line width of the MAS spectrum pertaining to **5**-^{15}N (Figure 3) cannot be primarily attributed to homonuclear couplings. An estimate of the contribution to the line width from irreversible dephasing and from imperfections due to the experimental implementation of the CPMG sequence is provided by a spin-echo spectrum of $Ta^{14}N_{0.76}{}^{15}N_{0.04}$ (**5′**-$^{15}N_{0.04}$), prepared from 95% $^{14}NH_3$/5% $^{15}NH_3$ and $(^tBuCH_2)_3Ta{=}CH^tBu$ (**1**, Scheme 2), where the ^{15}N is randomly distributed through the lattice. In this sample, the spin-echo signal decay was approximately exponential with an effective Lorentzian width of ~20 Hz (Table 1). Where line widths are observed that substantially exceed 20 Hz or are of obviously different line shape, the excess width is almost certainly associated with the short-range interactions that couple nuclear spins to one another.

Where only pairs of nuclear spins are present, the interpretation of the resulting spectra is relatively simple, e.g., where dipole−dipole couplings dominate, the distance in frequency between sharp features is directly interpretable in terms of an internuclear distance.[27,45] In more complex systems, or where the distribution of spin networks is inhomogeneous, such a simple interpretation is unavailable. Spectral simulations based on assumed cluster geometries may provide some clues. Often a spectrum is unstructured, hence estimation of the line width by second-moment calculations may be all that is justified. Without attempting a detailed calculation of the line shapes, the second moment of the ideal Ta^{15}N lattice of **5**-^{15}N was calculated by conventional methods for an assumed lattice (fcc, d(TaN) = 3.04 Å) with various numbers of nearest neighbors. Line-shape estimations of this type uniformly exceeded the experimental values, perhaps as a testament to the irregularity of the lattice, i.e., typical chemical shift differences exceeded typical dipole−dipole couplings. While the line widths were not accurately reproduced by the calculations, the closest were those that treated the spins as "unlike", as would be appropriate for a lattice containing numerous defects.

Despite the worrisome two-component feature observed in the spin-echo spectrum of Ta$^{15}N_{0.8}$ (**5**-^{15}N), it was hoped that more useful information might be derived from studies of dilute ^{15}N systems, where more structural dipolar lineshapes might be observed. Samples of 5% ^{15}N-pentamer-doped (**3′**-$^{15}N_{0.05}$, **4′**-$^{15}N_{0.05}$, **5′**-$^{15}N_{0.04}$) and 5%-^{15}N-random (**3**-$^{15}N_{0.05}$, **4**-$^{15}N_{0.05}$, **5**-$^{15}N_{0.04}$) oligomer, amorphous and cubic nitrides, prepared as indicated in Scheme 2, were subjected to spin-echo analysis (Table 1). In cases where doped samples exhibited significantly greater apparent line width than those of the random samples, local concentrations of ^{15}N would be implicated, and the precursor structure (i.e., the Ta_2N_2 "squares" of pentamer **2**) might directly correlate with fragments of the various solid-state species.

For **5**-$^{15}N_{0.04}$ and **5′**-$^{15}N_{0.04}$, virtually no difference was observed in the spin-echo spectra; in fact the line width of the random sample ($\nu_{1/2}$ = 21 Hz) was slightly greater than that of the doped material (18 Hz). The assumption of a static lattice of nitrogens in **5′**-$^{15}N_{0.04}$ is probably unrealistic,[46] especially given the nitrogen-deficient lattice generated at 820 °C; hence this result could still be consistent with a structural correlation that was obscured by ^{15}N/^{14}N scrambling in the doped sample. Undaunted, spin-echo spectra of **4**-$^{15}N_{0.05}$ vs **4′**-$^{15}N_{0.05}$ were obtained, because a structural correlation of the precursor with 400 °C amorphous material would still be compelling for several reasons: (1) at this stage in the scheme, virtually all volatiles have been lost; (2) electron diffraction suggests that crystalline regions are present; (3) interference from N diffusion is less likely during annealing at 400 °C for 24 h.[46] At first glance, the results for **4**/**4′**-$^{15}N_{0.05}$ (Figure 10) are provocative because the pentamer-doped sample shows significantly greater width (32 Hz (2048 transients), 42 Hz (8192 transients)) than that derived from randomly labeled starting material (25 Hz (2048 transients), 32 Hz (9642 transients)).

The data appear to provide direct evidence of the relationship of pentamer **2** to amorphous TaN (**4**) and hence cubic $TaN_{0.8}$ (**5**). However, several observations render the significance of this difficult to quantify. As suggested above, as signal-to-noise ratios increase (2K → 8−10K transients) for the same samples of **4′**-$^{15}N_{0.05}$ and the wide bases of the lines become better defined, the line widths appear consistently broader. Clearly, line widths and shapes can be best compared if signal-to-noise ratios are comparable. Furthermore, if the data for the amorphous material truly reflect local concentrations of ^{15}N for **4′**-$^{15}N_{0.05}$ vs **4**-$^{15}N_{0.05}$, spin-echo spectra of random vs pentamer-doped samples of the oligomeric precipitate **3** should surely manifest an obvious difference, yet the data are not supportive. The line width attributed to **3′**-$^{15}N_{0.05}$ (59 Hz, 1024 transients) is merely 4 Hz greater than that assigned to **3**-$^{15}N_{0.05}$ (55 Hz, 1024 transients).

This result was unexpected, since the aforementioned control experiments provided no evidence that loss of label from **2**-$^{15}N_5$—an obvious scrambling mechanism—was occurring, and the MAS results strongly implied

Table 1. Summary of Line Widths ($\nu_{1/2}$) Obtained from Spin−Echo Spectra of $1/n[TaC_{1.41}H_{3.90}N_{1.90}]_n$ (3), Amorphous TaN (4), and $TaN_{0.8}$ (5), When Prepared from 5% ^{15}N Randomly Doped and 5% 2-$^{15}N_5$-Doped (Primed) Samples According to Scheme 2

sample	$\nu_{1/2}$	transients	dwell time (μs)
3-$^{15}N_{0.05}$	55	1024	100
3′-$^{15}N_{0.05}$	59	1024	100
4-$^{15}N_{0.05}$	25	2048	200
4′-$^{15}N_{0.05}$	32	2048	200
4-$^{15}N_{0.05}$[a]	32	9642	200
4′-$^{15}N_{0.05}$[a]	42	8192	200
5-$^{15}N_{0.04}$[b]	21	1368	100
5′-$^{15}N_{0.04}$[b]	18	1212	100

[a] Spectra were aquired seven molecular orbitals subsequent to the previous ones, but spectral evidence of decomposition was not evident. [b] Subscript reflects the 20% nitrogen vacancies attributed to the cubic nitride.

(45) (a) Yannoni, C. S.; Bernier, P. P.; Bethune, D. S.; Meijer, G.; Salem, J. R. *J. Am. Chem. Soc.* **1991**, *113*, 3190−3192. (b) Pake, G. E. *J. Chem. Phys.* **1948**, *16*, 327.

(46) Examination of diffusion rate for related oxide complexes suggests that nitrogen diffusion in $TaN_{0.8}$ (**5**) quite plausibly occurs on the time scale of annealing (72 h) at 800 °C but is far less likely to occur during the formation (24 h, 400 °C) of amorphous TaN (**4**). See: Kingery, W. D.; Bowen, H. K.; Ulmann, D. R. *Introduction to Ceramics*, 2nd ed.; John Wiley & Sons: New York, 1976.

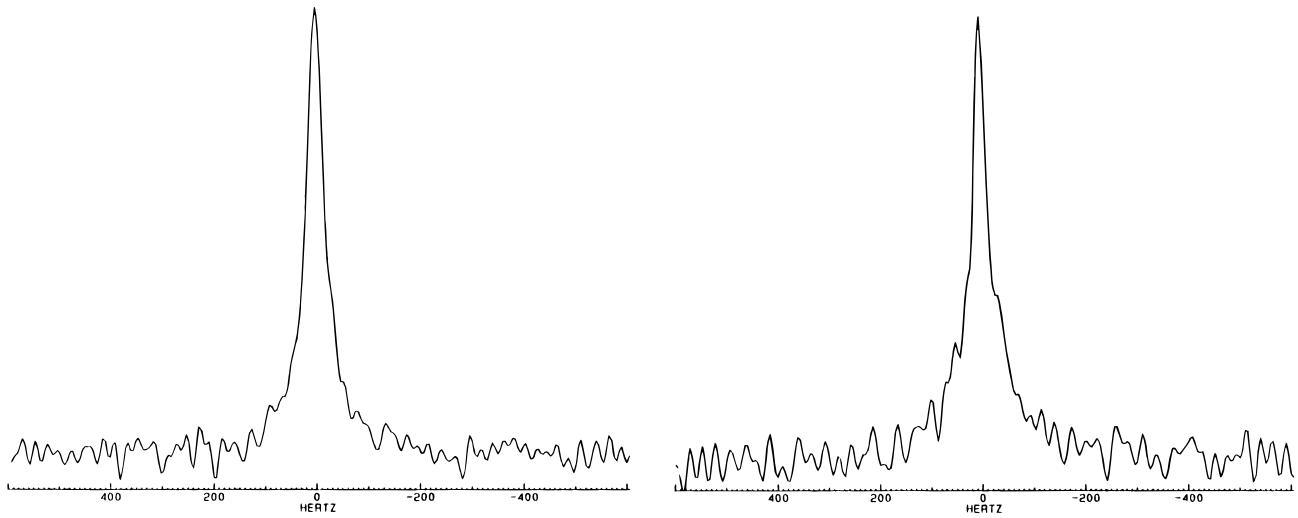

Figure 10. Spin−echo (CPMG sequence) spectra of amorphous $Ta^{15}N_{0.05}$ (**4′**-^{15}N) derived from 95% $[(^tBuCH_2)_2TaN]_5$ (**2**) and 5% $[(^tBuCH_2)_2Ta^{15}N]_5$ (**2**-$^{15}N_5$) (left, 42 Hz line width (8192 transients)) and randomly labeled amorphous $Ta^{15}N_{0.05}$ (**4**-^{15}N) derived from $(^tBuCH_2)_3Ta{=}CH^tBu$ (**1**) and 95% $^{15}NH_3$/5% NH_3 (right, 32 Hz line width, 9642 transients). See Scheme 2 for details.

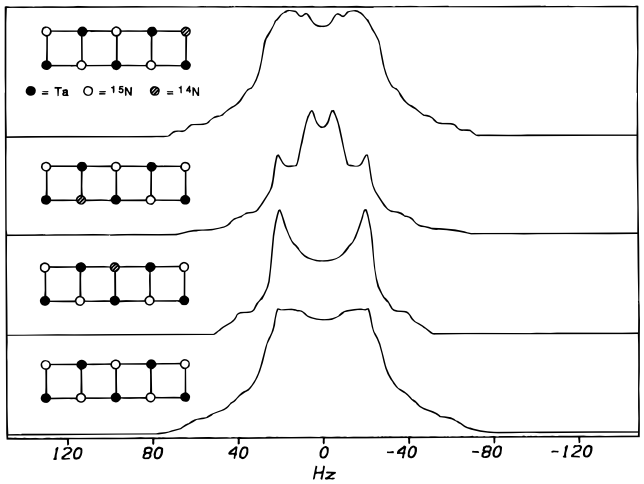

Figure 11. Calculated spin−echo spectra of three four-spin networks and one five-spin network; each specific network is illustrated.

that condensation of the pentamer ladders leads to **3**. Unfortunately, spin-echo spectra of **3**/**3′**-$^{15}N_{0.05}$ may not be an appropriate model because of the added complexity of the material, which contains various types of nitride, amide, imide(?), and ammonia sites. Since the dilute (i.e., randomly doped) sample **3**-$^{15}N_{0.05}$ should reflect the intrinsic line width of an "average" ^{15}N in the material, it and the corresponding pentamer-doped sample cannot be compared to **4**/**4′**-$^{15}N_{0.05}$.

In each sample, the spectral line shape was decidedly non-Lorentzian, as is expected when the dipolar fields between sites are effective. To obtain a better understanding of how localized distributions of small numbers of ^{15}N sites would appear, spectra of four neighboring ^{15}N nuclei have been calculated in various patterns as shown in Figure 11. The ^{15}N nuclei were calculated at distances consistent with those expected for TaN, are weakly coupled to one another with chemical shift differences suppressed, and are assumed to be in a "powder pattern" distribution corresponding to a disordered sample, thereby mimicking a spin-echo spectrum. Naturally, the real spectrum would consist of a number of overlapping patterns corresponding to a distribution of ^{15}N networks. Morover, while networks of four spins were arbitrarily chosen for the calculation, there would be additional networks with different numbers of spins, and a narrower component representing the ^{15}N nuclear spins that have migrated out of the denser networks. Much of the critical information necessary to identify the nature of the surviving networks resides in the basal portion of the spectrum—exactly that part of the spectrum most greatly effected by signal-to-noise difficulties. Clearly, a greater doping percentage would have provided greater intensity. Since the spectra most certainly reflect a variety of ^{15}N patterns—whether in the random or doped samples—the apparent line widths at half-maximum were as good a parameter for comparison as any, but such an approach must obviously be cautiously treated.

In summary, while it is tempting to conclude that there exists a direct link between pentamer **2** and amorphous TaN (**4**) based on the above spin-echo solid-state NMR analysis, prudence dictates that this inference is extremely tenuous. It is reasonably safe to conclude that scrambling of ^{15}N label occurs prior to or during the annealing to give $TaN_{0.76}{}^{15}N_{0.04}$ (**5′**-$^{15}N_{0.04}$), but this result is predictable in any case from estimates of nitrogen-diffusion rates, especially in an N-deficient lattice.[46]

Conclusions

Solid-state ^{15}N NMR is clearly a noninvasive, informative tool for observing the transformation of a molecular precursor to a solid-state material. In particular, the MAS spectra, provided that they are appropriately calibrated with relevant solution or solid knowns, may be straightforwardly interpreted to gain information about the course of reaction. In the above tantalum nitride case, the spectral information meshes well with elemental and other analyses to provide a substantive model.

While the MAS spectra are relatively easy to interpret and reconcile with auxiliary data for the purpose of characterization, the spin-echo experiments were designed as a mechanistic probe in the hope of providing evidence of a direct relationship between the pentameric molecular precursor, $[(^tBuCH_2)_2TaN]_5$ (**2**), to the

nitrogen-deficient cubic nitride, $TaN_{0.8}$ (**5**). Unfortunately, while hints of such a relationship were realized, the experiments fall short of being conclusive, partly due to the nature of the system, and partly due to difficulties inherent to interpretation and acquisition of the spectra. For instance, while the intrinsic line width of $TaN_{0.76}{}^{15}N_{0.04}$, which serves as a dilute sample, is around 20 Hz, additional broadening due to first-order dipolar and *J* coupling results only in additional broadening on the order of 35 Hz, as evidenced in the spin-echo spectrum of $Ta^{15}N_{0.8}$ (**5**-^{15}N). Therefore, in order to use the line widths derived from random vs pentamer-doped samples as an indicator of local ^{15}N concentration, the data must be quite precise. Since the nearest neighbor $^{15}N\cdots{}^{15}N$ interaction is ~3.04 Å, a substantial distance, the maximum amount of broadening due to homonuclear dipolar and *J* coupling, as manifested by 98% labled **5**-^{15}N is relatively small. Unfortunately, the spin echo experiments are time-consuming, and signal/noise problems can severely limit the precision of the measurements.

The ambiguous results regarding differences in the random vs pentamer-doped **4**/**4′**-$^{15}N_{0.05}$ suggest that a greater number of spin-echo experiments need be performed in order to ensure believability. For future applications, it is suggested that the percent random and precursor doping be varied, and the spectra of all samples be obtained using a uniform set of aquisition parameters. In this fashion a percent precursor doping vs line width curve can be evaluated with respect to a calibration line of percent random doping vs line width. Such a set of experiments would also permit—in the occurrence of an observable deviation between nonrandomly and randomly generated samples—an estimate of the local concentration of ^{15}N in the nonrandomly generated material from comparison of the line widths of the varied percentages of randomly prepared solids. In any event, the labeling/spin-echo experiments still show promise but are probably best applied to simple solids (i.e., where the homonuclear atom-atom distance is short) where the spin−spin interactions are known or readily calculable from structural studies.

Finally, the above analysis ignores the possibility that trace amounts of carbide may pin the structure of TaN to the cubic phase.[14,23] It is impossible to disprove the carbide pinning mechanism because analytical methods to detect carbon in trace quantities within a solid are not accurate enough to satisfactorily dispel this notion. As a consequence, all of the data presented above were collected and interpreted with the full knowledge that a carbide pinning mechanism would always be a plausible alternative. It is worth noting that if carbide is present, it must not be substantially altering the thermodynamics of the system, because $TaN_{0.8}$ (**5**) was readily converted to the more stable hexagonal phase (**6**) upon thermolysis for 24 h at 1100 °C (Scheme 1). Without this observation, the mechanistic probes delineated above would not have been attempted.

Experimental Section

General Considerations. All manipulations were performed with use of either glovebox or high-vacuum line techniques. Ethereal and hydrocarbon solvents were distilled under nitrogen from purple benzophenone ketyl and vacuum transferred from the same prior to use. Small amounts of tetraglyme (2−5 mL/L solvent) were added to hydrocarbons to solubilize the ketyl. Benzene-d_6 was dried over sodium, activated 4 Å molecular sieves, vacuum transferred, and stored under N_2; THF-d_8 was dried over sodium benzophenone ketyl. Anhydrous ammonia was purchased from Matheson. $^{15}NH_3$ (Aldrich) was degassed via freeze−pump−thaw cycles and dried over sodium. $(^tBuCH_2)_3Ta{=}CH^tBu$ (**1**)[28] and $^tBuNTa(NMe_2)_3$ (**9**)[30] were prepared via literature methods, while a modified synthesis of $Ta(NMe_2)_5$ (**7**)[29] was developed.

Solution ^{15}N spectra were obtained using a Varian XL-400 (^{15}N) spectrometer and referenced to natural abundance CH_3NO_2 (neat, δ 0.00)[27,36] using a coaxial 5 mm tube containing the lock solvent; a delay of 40 s and a pulse width of 30° were employed. Solid-state ^{15}N MAS NMR spectra were obtained at Cornell using an IBM NR/300 spectrometer fitted with an IBM solids rack and Doty Scientific Inc. solids probes. All ^{15}N spin-echo spectra as well as some ^{15}N and ^{13}C MAS and CPMAS spectra were obtained using Bruker 300 or 400 MHz MSL spectrometers at Bruker Instruments, Inc., Boston, MA. Solid ^{15}N spectra were initially referenced to solid, external $^{15}NH_4Cl$ but are reported referenced to neat nitromethane for correlation to solution data (δ(referred to NH_4Cl) − 341(1) = δ(referred to CH_3NO_2)).[27,36] Infrared spectra were recorded on a Mattson FT-IR or Perkin-Elmer 299B grating IR. FAB mass spectra were obtained on a Kratos MS89OMS or Finnegan MAT delta S spectrometers. Magnetic susceptibility measurements (5−250 K) were made using a Faraday balance; corrections for diamagnetism were estimated from Pascal's constants.[47] Electron microscopy (JEOL 200CX STEM) was used to confirm the uniformity of amorphous TaN (**4**). Analyses were obtained by Oneida Research Services, Whitesboro, NY.

Procedures. *1. Ammonolysis of solid $(^tBuCH_2)_3Ta{=}CH^tBu$ (**1**).* An alumina boat was charged with 1.025 g (2.207 mmol) of $(^tBuCH_2)_3Ta{=}CH^tBu$ (**1**) and heated in a quartz tube with an alumina boat containing Ti foil placed upstream. A 2000 mL flask containing a mixture of NH_3(l) and sodium metal was attached to the stainless steel endpieces fitted to the quartz tube and purged through a T valve. After 1.5 h the solid was exposed to the flowing ammonia, and the solid formed an oil. The reaction was allowed to proceed at ambient temperature for 1 h at which time the liquid present in the boat was heated to 50 °C causing it to boil. One hour later boiling had ceased and the green-black solid was heated to 100 °C generating a red solid. Further heating for 2 days at 800 °C resulted in 316 mg of silvery-red solid. XRD showed this material to contain *Fm*3*m* TaN, Ta_3N_5, and numerous other products.

*2. Synthesis of cubic TaN (**5**) from $Ta(NMe_2)_5$ (**7**).* A 50 mL flask was charged with 2.593 g of $Ta(NMe_2)_5$ (**7**) and evacuated, and 30 mL of hexane introduced by distillation. The solution was cooled to −78 °C, stirred, and exposed to an excess of NH_3. A yellow solid quickly precipitated, and the mixture was allowed to warm to room temperature. The mixture was vented to a bubbler so that the excess NH_3 and Me_2NH could boil off. After 2 h the solid was filtered and all volatiles removed giving 1.23 g of an insoluble, amorphous solid (**8**). The solid was annealed according to the procedure previously delineated,[13] resulting in a 14% weight loss and a jet black solid by 400 °C. Further heating to 800 °C resulted in an additional 9.4% weight loss and the formation of cubic TaN (*Fm*3*m*, a = 4.310(2) Å) with 5% of unidentified impurities.

*3. Synthesis of Cubic TaN from $^tBuNTa(NMe_2)_3$ (**9**).* A 100 mL flask was charged with 1.127 g of $^tBuNTa(NMe_2)_3$ (**9**) and evacuated, and 40 mL of hexane introduced via distillation. The stirred solution at 20 °C was exposed to 1 atm of NH_3. After 4 h a yellow precipitate had formed, all volatiles were stripped, and the material was isolated as 0.779 g of a deep yellow, glassy solid. The solid was annealed according to the procedure previously delineated,[13] resulting in a 36% weight loss and a jet-black, shiny, amorphous (by XRD) solid by 400 °C. Upon heating to 600 °C for 42 h no further weight loss

(47) Lewis, J.; Wilkins, R. C. *Modern Coordination Chemistry*; Wiley Interscience: New York, 1960; p 403.

occurred but the sample remained amorphous. Additional annealing at 950 °C for 4 days gave clean, but poorly crystalline *Fm*3*m* TaN.

*4. Nitrogen Analysis of Cubic (**5**) and Hexagonal (6) TaN_{1-x}.* A 54 mg sample of cubic TaN was added to a 25 mL Erlenmyer flask containing 5 mL 85% phosphoric acid and 0.7024 g of $SnCl_2 \cdot H_2O$. The sample was boiled on a hot plate until water vapor was no longer apparent over the solution. The sample was then heated over a Bunsen burner until gray phosphate precipitates had formed. Calibrant solutions containing 0, 20, 30, and 40 ppm $(NH_4)_2SO_4$ in the matrix of 85% H_3PO_4 and $SnCl_2 \cdot H2O$ were treated to the same heating conditions. These solutions all deposited the expected milky white phosphate precipitates. The samples were diluted to 50.0 mL. The ammonium concentration was determined via addition of 0.15 mL of the solution of interest to 2.0 mL of a solution of 8.5% sodium salicylate and 0.03% sodium nitroferricyanide. Color development was initiated by the addition of 2.0 mL each of 1.5 g/L sodium dichloroisocyanurate and 48 g/L sodium hydroxide. Color development was complete within 1/2 h. The sample were then diluted with 20.0 mL distilled water and read at 660 nm using a 10 mm flow through cell. Both hexagonal ($P\bar{6}2m$) and cubic (*Fm*3*m*) tantalum nitride were analyzed. The gray color of the phosphate precipitates is probably indicative of incomplete reaction so the values provide lower limits of nitrogen. Compositions of cubic (*Fm*3*m*) $TaN_{0.80}$ (**5**) and Aldrich hexagonal ($P\bar{6}2m$) $TaN_{0.95}$ (**6**) were determined.

*5. Solution Integrity of $[(^tBuCH_2)_2TaN]_5$ (**2**).* An NMR tube was charged with 17 mg (0.0091 mmol) of $[(^tBuCH_2)_2Ta^{15}N]_5$ (**2**-^{15}N) and 0.3 mL of benzene-d_6 added via distilliation. NH_3 (0.046 mmol, 5 equiv) was condensed into the tube, which was then flame sealed. The mixture was monitored via solution ^{15}N NMR until the color had changed from yellow to brown-black and precipitate had formed. No evidence of ^{15}N ammonia or washing out of pentamer peaks occurred during this time.

*6. Synthesis of random 5% ^{15}N-labeled **2**−**5**.* A 400 mL glass bomb reactor was charged with 2.060 g (4.435 mmol) of $(^tBuCH_2)_3Ta{=}CH^tBu$ (**1**) and evacuated, and 100 mL of benzene introduced via distillation. Ammonia ($^{14}NH_3$, 8.43 mmol, 1.9 equiv; $^{15}NH_3$, 0.444 mmol, 0.10 equiv) was condensed into the flask at 77 K in two portions, and the mixture was allowed to warm. Green-orange **2** (0.964 g) was generated according to previous procedures, which were also followed to produce **3**−**5**.[13]

Extended Hückel Molecular Orbital Calculations. All EHMO calculations were performed with parameters and methods previously described.[13]

Acknowledgment. Financial support from the Air Force Office of Scientific Research and the Materials Science Center at Cornell University, as well as fellowship support from IBM (M.M.B.H.) is gratefully acknowledged. We thank Bruker Instruments, Inc., Boston, MA, for providing generous spectrometer time for the solid-state MAS and spin-echo measurements. Dr. Douglas Burum (Bruker) is acknowledged for important discussions regarding the spin-echo experiments.

CM960034Z